

Specific Features of $\text{Li}_5\text{La}_3\text{M}_2\text{O}_{12}$ ($\text{M} = \text{Nb}, \text{Ta}$) Single Crystals: Electrolyte for Solid States Batteries

Wilayat Khan^{1,*} and A. H. Reshak^{1,2}

¹New Technologies-Research Center, University of West Bohemia, Univerzitni 8, 30614 Pilsen, Czech Republic

²Center of Excellence Geopolymer and Green Technology, School of Material Engineering, University Malaysia Perlis, 01007 Kangar, Perlis, Malaysia

ABSTRACT

Density functional theory and Boltzmann transport equations are employed to calculate the thermoelectric transport coefficients, electronic structure and optical properties of bulk garnet-like oxides $\text{Li}_5\text{La}_3\text{M}_2\text{O}_{12}$ ($\text{M} = \text{Nb}, \text{Ta}$) single crystals. The calculated energy band structure and density of states disclose a metallic nature for both compounds. $\text{Li}_5\text{La}_3\text{Nb}_2\text{O}_{12}$ possesses a greater density of states around Fermi level than $\text{Li}_5\text{La}_3\text{Ta}_2\text{O}_{12}$, which is due to the Nb/Ta-d states. The calculated electronic charge density of both compounds indicates a dominant ionic character of chemical bonding. Optical susceptibilities, including the real and imaginary parts of the optical dielectric functions, reflectivity and energy loss function, are calculated. The reflectivity of the investigated compounds reaches 60% in the UV region. The maximum peaks in the energy loss function are due to the plasmon resonance with the decreasing energy of electrons instead of surface plasmon loss. The Seebeck coefficients, power factor, figure of merit, heat capacity as well as electrical and thermal conductivities are calculated as a function of temperature for relaxed structures, using BoltzTraP code at constant pressure, which strongly affected by carrier and intrinsic defects concentration. Our calculated result shows that $\text{Li}_5\text{La}_3\text{Ta}_2\text{O}_{12}$ is better than $\text{Li}_5\text{La}_3\text{Nb}_2\text{O}_{12}$ along the entire temperature ranges.

KEYWORDS: Electronic Structure, Electronic Charge Density, Optical Properties, Thermoelectric Properties, DFT, EVGGA.

1. INTRODUCTION

The improvement of solid Li ion electrolytes with appropriate useful properties is of considerable scientific interest due to the variety of possible electrochemical applications, for example, in solid-state batteries, sensors, and electrochromic displays.^{1,2} In this regard, some Li encompassing metal oxides have been discovered recently. However, lithium lanthanum titanate (LLT) is not preferred choice as an electrolyte in high energy density batteries, which instead use lithium metal anode. This is attributed to the fact that LLT is unstable in direct contact with the lithium element and undergoes fast Li insertion, with the consequent reduction of Ti^{4+} to Ti^{3+} , thus leading to greater electronic conductivity. Conversely, the LLT is restricted to use as an electrode material, due to the minor Li uptake.^{3–5}

Up to now, it has been reported^{1,6,7} that in some crystalline and amorphous compounds which consist of polyanions, like SiO_4^{4-} or PO_4^{3-} , such as Li_4SiO_4 and Li_3PO_4 and other compounds with similar structure, exhibit high Li

ion conductivity plus chemical and electrochemical stability. In recent times, Thangadurai et al.⁸ reported fast conductivity of Li ions in metal oxides containing Li with minor side formation of $\text{Li}_5\text{La}_3\text{M}_2\text{O}_{12}$ (where $\text{M} = \text{Nb}, \text{Ta}$, these are symmetrically related to the garnet symmetry). The above mentioned oxides have been identified on examining the ternary structure figure of $\text{La}_2\text{O}_3\text{--M}_2\text{O}_5\text{--Li}_2\text{O}$.^{9,10} Both aforementioned oxides ($\text{Li}_5\text{La}_3\text{Nb}_2\text{O}_{12}$ and $\text{Li}_5\text{La}_3\text{Ta}_2\text{O}_{12}$) possess similar volumetric Li ions conductivity of the order of 10^{-6} S/cm at 298 K with E_A (activation energy) of 0.43 and 0.56 eV, respectively.⁹ In comparison, the Ta atom in $\text{Li}_5\text{La}_3\text{Ta}_2\text{O}_{12}$ compound has attracted special curiosity as an electrolyte substance used in solid state batteries because of its stability against reaction with liquefied Li. For the first time these compounds in garnet-like symmetry have been recently used in fast Li ion conductivity, thus opening a new research area for the optimized conductivity due to the modifications in the structure. Thangadurai et al.¹¹ used the bond valence misalliance measurement analysis to evaluate the chemical plausibility of the published symmetry models and clarify possible routes for the motion of Li^+ in both compounds (the distinguishing features of the three-dimensional Li-pathway network is a non-planar square of Li positions).

* Author to whom correspondence should be addressed.

Email: walyat76@gmail.com

Received: xx xx xxxx

Accepted: xx xx xxxx

Herein, we suggest a new class of materials with better thermoelectric power factor by employing the Boltzmann transport technique¹² and the density functional theory (DFT)¹³ for calculating the electronic structure, electronic charge density and optical properties for $\text{Li}_5\text{La}_3\text{Nb}_2\text{O}_{12}$ (LLNO) and $\text{Li}_5\text{La}_3\text{Ta}_2\text{O}_{12}$ (LLTO) compounds. The optical properties are explained on the basis of band structure (BS) and density of states (DOS), and the effect of Nb and Ta concentrations on the power factor, which is key for thermoelectric devices such as batteries, is discussed.

2. CALCULATION METHODS

The calculation was performed within the framework of density functional theory (DFT),¹³ using the full-potential linearized augmented plane-wave (FP-LAPW) method, as employed in the WIEN2K computer package.^{14,15} In our calculation, the exchange co-relation (XC) potential was computed by mean of local density approximation (LDA),¹⁶ generalized gradient approximation (GGA)¹⁷ and Engel-Vosko generalized gradient approximation (EVGGA),¹⁸ the latter giving better results as compared to the other approximations. The atomic Muffin-Tin (MT) sphere radii are chosen in such a way that there is no overlapping between the spheres. The MT sphere radii are $R_{\text{MT}}(\text{La}) = 2.40$ a.u., $R_{\text{MT}}(\text{Ta}) = 2.02$ a.u., $R_{\text{MT}}(\text{Li}) = 1.72$ a.u. and $R_{\text{MT}}(\text{O}) = 1.72$ a.u. of LLTO compound, while for LLNO compound the radii are $R_{\text{MT}}(\text{La}) = 2.25$ a.u., $R_{\text{MT}}(\text{Nb}) = 1.86$ a.u., $R_{\text{MT}}(\text{Li}) = 1.72$ a.u. and $R_{\text{MT}}(\text{O}) = 1.65$ a.u., respectively. The cut-off energy ($R_{\text{MT}}K_{\text{MAX}}$), which separates the valence and core states, is chosen to be about 6.0, where R_{MT} represents the smallest atomic sphere radii in the unit cell and the parameter K_{MAX} represents the maximum value of the reciprocal lattice vector (used to expand the plane wave). The term G_{max} stands for maximum charge density cut-off, which is about of 12.0 a.u.^{-1} . When the energy difference between the input and output energy per formula unit is smaller than 10^{-4}

Ryd, then the self consistence calculations are obtained. The structure of bulk Garnet-like oxides $\text{Li}_5\text{La}_3\text{Nb}_2\text{O}_{12}$ (LLNO) and $\text{Li}_5\text{La}_3\text{Ta}_2\text{O}_{12}$ (LLTO) is cubic with space group $Ia-3$ (# 206). The optimized crystal structures are illustrated in Figures 1(a), (b). The atomic positions and lattice constants are listed in the Table I, and compared with the experimental data.⁵

The electronic transport properties are calculated on the basis of Boltzmann theory as employed in BoltzTraP code. The Boltzmann transport relations are used to explain the variation of electrons/holes distribution in the real compounds.

Using this technique, the Seebeck coefficient, electrical/thermal conductivities, power factor and figure of merit are computed under constant relaxation time (energy dependent) to estimate the electronic transport performance of some thermoelectric materials. Mathematically, the electronic transport tensors as a function of temperature and chemical potential,¹⁹⁻²¹ can be expressed as;

$$\sigma_{\alpha\beta}(\mu, T) = \frac{1}{\Omega} \int \bar{\sigma}_{\alpha\beta}(\varepsilon) \left[-\frac{\partial f_0(T, \varepsilon, \mu)}{\partial \varepsilon} \right] d\varepsilon \quad (1)$$

$$S_{\alpha\beta}(\mu, T) = \frac{1}{eT\Omega\sigma_{\alpha\beta}(T, \mu)} \times \int \bar{\sigma}_{\alpha\beta}(\varepsilon)(\varepsilon - \mu) \left[-\frac{\partial f_0(T, \varepsilon, \mu)}{\partial \varepsilon} \right] d\varepsilon \quad (2)$$

where the terms α and β are the tensor subscripts, and Ω , μ and f_0 represent the volume of the unit cell, Fermi level of charge carriers, and Fermi distribution function, respectively. The $\sigma_{\alpha\beta}$ (conductivity distribution), which is very important part of σ , is given by;

$$\bar{\sigma}_{\alpha\beta} = \frac{e^2}{N} \sum_{i,k} \tau \cdot v_{\alpha}(i, k) \cdot v_{\beta}(i, k) \cdot \frac{\delta(\varepsilon - \varepsilon_{i,k})}{d\varepsilon} \quad (3)$$

In the above equation, the wave vector, band indices, and number of k points are symbolized by k , i and N ,

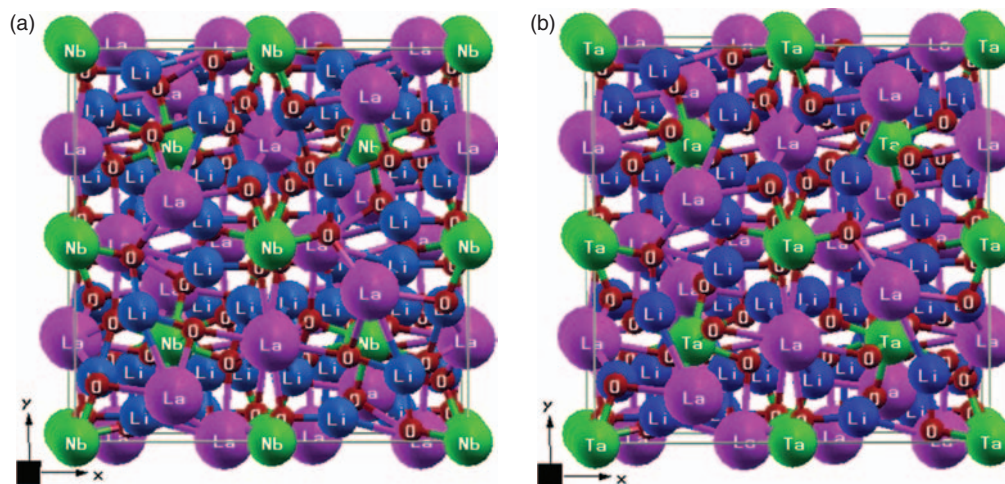


Fig. 1. Molecular structure of $\text{Li}_5\text{La}_3\text{Nb}_2\text{O}_{12}$ and $\text{Li}_5\text{La}_3\text{Ta}_2\text{O}_{12}$.

Table I. Lattice constant and atomic position of $\text{Li}_5\text{La}_3\text{Nb}_2\text{O}_{12}$ and $\text{Li}_5\text{La}_3\text{Ta}_2\text{O}_{12}$.

$\text{Li}_5\text{La}_3\text{Nb}_2\text{O}_{12}$							
$A(\text{\AA})$		12.826 _(Exp)			12.736 _(Opt)		
Lattice parameters	Atoms	x (Exp)	y (Exp)	z (Exp)	x (opt.)	y (opt.)	z (opt.)
Atomic co-ordinates	La	0.1264	0	1/4	0.1137	0	1/4
	Nb	0	0	0	0	0	0
	Nb	1/4	1/4	1/4	1/4	1/4	1/4
	Li	0.6318	0.3244	0.5814	0.6608	0.3297	0.5584
	O	0.2802	0.1012	0.2260	0.2836	0.1020	0.1979
O	0.3637	0.5264	0.4346	0.3549	0.5288	0.4434	
$\text{Li}_5\text{La}_3\text{Ta}_2\text{O}_{12}$							
$A(\text{\AA})$		12.829 _(Exp)			12.739 _(Opt)		
Lattice parameters	Atoms	x (Exp)	y (Exp)	z (Exp)	x (opt.)	y (opt.)	z (opt.)
Atomic co-ordinates	La	0.1267	0	1/4	0.1196	0	1/4
	Ta	0	0	0	0	0	0
	Ta	1/4	1/4	1/4	1/4	1/4	1/4
	Li	0.6312	0.3237	0.5824	0.6533	0.3302	0.5599
	O	0.2795	0.1011	0.2267	0.2866	0.1051	0.1977
O	0.3639	0.5273	0.4349	0.3538	0.5275	0.4472	

respectively. $v_\alpha/v_\beta(i, k)$ represent the α/β components of the group velocity $v(i, k)$ of charge carrier. The group velocity $v(i, k)$ is formulated as;

$$v(i, k) = \frac{1}{\hbar} \frac{\partial \varepsilon(i, k)}{\partial k_\alpha} \quad (4)$$

This velocity is calculated from the energy band structures, also called band crossing.²⁵ In this theory, the mobility of electrons is treated semiclassically. The temperature and chemical potential dependent thermal conductivity tensor can be written as;

$$\kappa_{\alpha\beta}(\mu, T) = \frac{1}{eT\Omega} \times \int \sigma_{\alpha\beta}(\varepsilon)(\varepsilon - \mu)^2 \left[-\frac{\partial f_0(T, \varepsilon, \mu)}{\partial \varepsilon} \right] d\varepsilon \quad (5)$$

The electronic thermal conductivity is computed as:

$$\kappa_e = \kappa^0 - S^2\sigma T \quad (6)$$

It has been found that these electronic transport coefficients are linked to the integral of zero-, first- and second-order moments of the above tensor. Finally, from the solution of the above equation, we can obtain the power factor ($S^2\sigma$) and figure of merit ($ZT = S^2\sigma T/\kappa$), which provide information about the material efficiency.

3. RESULTS AND DISCUSSION

3.1. Electronic Structure

In order to discuss the optical properties of a material, it is necessary to investigate the electronic structure. The band

structures of LLTO and LLNO single crystals, calculated along high symmetry directions of the irreducible Brillouin zone (IBZ) using EVGGA, are presented in Figures 2(a), (b). The arrangement of energies of the conduction band (CB) and valence band (VB) are performed in such a manner that the Fermi energy level is assigned to the zero energy (shown by dotted lines). Figures 2(a), (b) shows considerable overlapping between the valence and conduction bands, which confirms the metallic nature of both compounds (LLTO and LLNO). One can see from Figures 2(a), (b), that the bands crossing the Fermi level E_F belong to Nb-d states of LLNO compound and Ta-d states of LLTO compound.

The calculated total density of states (TDOS) and partial density of states (PDOS) of our investigated Nb doped compound LLNO and Ta doped compound LLTO obviously explain the electronic states of the different atoms that contributed to the total density of states, as shown in Figures 3(a)–(i). As there is no band gap for these compounds, the TDOS shows a value of density of states at the Fermi level, E_F .

The magnitude of TDOS for LLNO compound are higher than that of LLTO compound. On moving from LLNO compound to LLTO compound, the TDOS is shifted toward lower energy, as illustrated in Figure 3, which suggests that the spectrum extended from -20.0 eV to 10.0 eV can be divided into four regions. One can notice that the electronic states (d-states) of Nb and Ta atoms give greater contribution than other states of different atoms, which are positioned at energy ranging from -20.0 eV to -15.0 eV. The energy region from -10.0 eV to -5.0 eV, mainly originates from O-p state in both

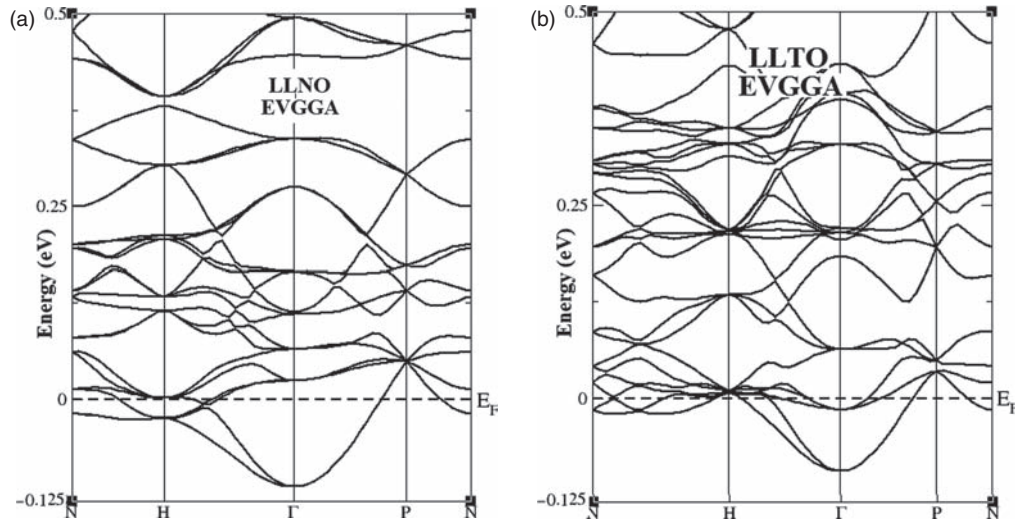


Fig. 2. Calculated band structure of $\text{Li}_5\text{La}_3\text{Nb}_2\text{O}_{12}$ and $\text{Li}_5\text{La}_3\text{Ta}_2\text{O}_{12}$, using EVGGA.

compounds (Fig. 3(g)), and the same behavior of O-p state are also observed in the region from -5.0 eV to 0.0 eV. This could elucidate various properties of both Nb doped and Ta doped compounds. Above the Fermi level from 0.0 to 10.0 eV, La-f state shows a larger contribution with the La-p and Ta/Nb-d states, while the La-s, Ta-f, Ta/Nb-s/p and Li-s states give a small contribution to density of states. Overall, the states belonging to LLNO compound give a strong contribution, as compared to the states of LLTO compound.

The calculated values of total density of states at Fermi level E_F , $N(E_F)$, for both compounds LLNO and LLTO using LDA, GGA and EVGGA, are listed in Table II, in which LLNO is predicted to have greater value of $N(E_F)$ than that of LLTO. For both compounds, the bar electronic specific heat co-efficient (γ), which depend on the density of states, is calculated using the following expression:

$$\gamma = \frac{1}{3} \pi^2 N(E_F) K_B^2 \quad (7)$$

where $N(E_F)$ represents the total density of states at the Fermi energy (E_F) and K_B represents the Boltzmann constant. By using the values of calculated density of states $N(E_F)$, we can obtain the bare electronic specific heat coefficient (γ) for both compounds LLNO and LLTO, which are given in Table II.

The electronic charge density is a very important parameter to explain the bonding nature, bonding properties, and the transfer of charge from one atom to another atom. We calculate the electronic charge density for both compounds in (100) and (010) crystallographic planes, using EVGGA exchange correlation functional, as illustrated in Figures 4(a)–(d). The electronegativity (EN) values for Li, La, Nb, Ta and O atoms are 0.98, 1.10, 1.60, 1.50 and 3.44, respectively. One can see from Figure 4, that the oxygen atom is surrounded by spherical lines, which indicate

the dominance of ionic character of chemical bonding. The nature of chemical bonding is obtained from the electronegativity difference. Lanthanum and oxygen atoms have electronegativity difference of 2.34, which predicts strong ionic bonding between them, with charge being attracted toward from lanthanum to oxygen atom because of its high electronegativity. An ionic bond is also found between oxygen and niobium atoms, because of high electronegativity difference of about 1.84. According to thermo-scale, the blue color indicates maximum concentration of charge around the atomic site, while the red color shows zero concentration. One can see from Figure 4, that strong sharing of electrons between oxygen and tantalum atoms. We should emphasize that only three atoms contribute to the charge density in the (100) plane, but all atoms provide contributions to the (010) plane. Our calculated bond lengths of $\text{Li}_5\text{La}_3\text{Nb}_2\text{O}_{12}$ compound are listed in Table III. Our results indicate close agreement with the experiments,⁵ which prove the accuracy of our calculations based on EVGGA exchange correlation potential.

3.2. Optical Properties

We have calculated the linear optical properties of both compounds (LLNO and LLTO) in the cubic symmetry. The complex dielectric (frequency dependent) tensor $\epsilon(\omega)$, accounting for intra/inter-band transitions, was calculated within the random phase approximation based on the calculated band structure. The calculated imaginary parts $\epsilon_2(\omega)$ of the dielectric tensor as a function of photon energy $\hbar\omega$ of both compounds are plotted in the 0.0 – 0.8 eV energy range in Figure 5(a). A considerable dispersion is found for the imaginary part $\epsilon_2(\omega)$ of dielectric tensor of both compounds. There are two types of optical transitions which are contributing to the spectra of the imaginary part $\epsilon_2(\omega)$, namely, the intra- and inter-band transitions. From Figure 5(a) it is clear that the

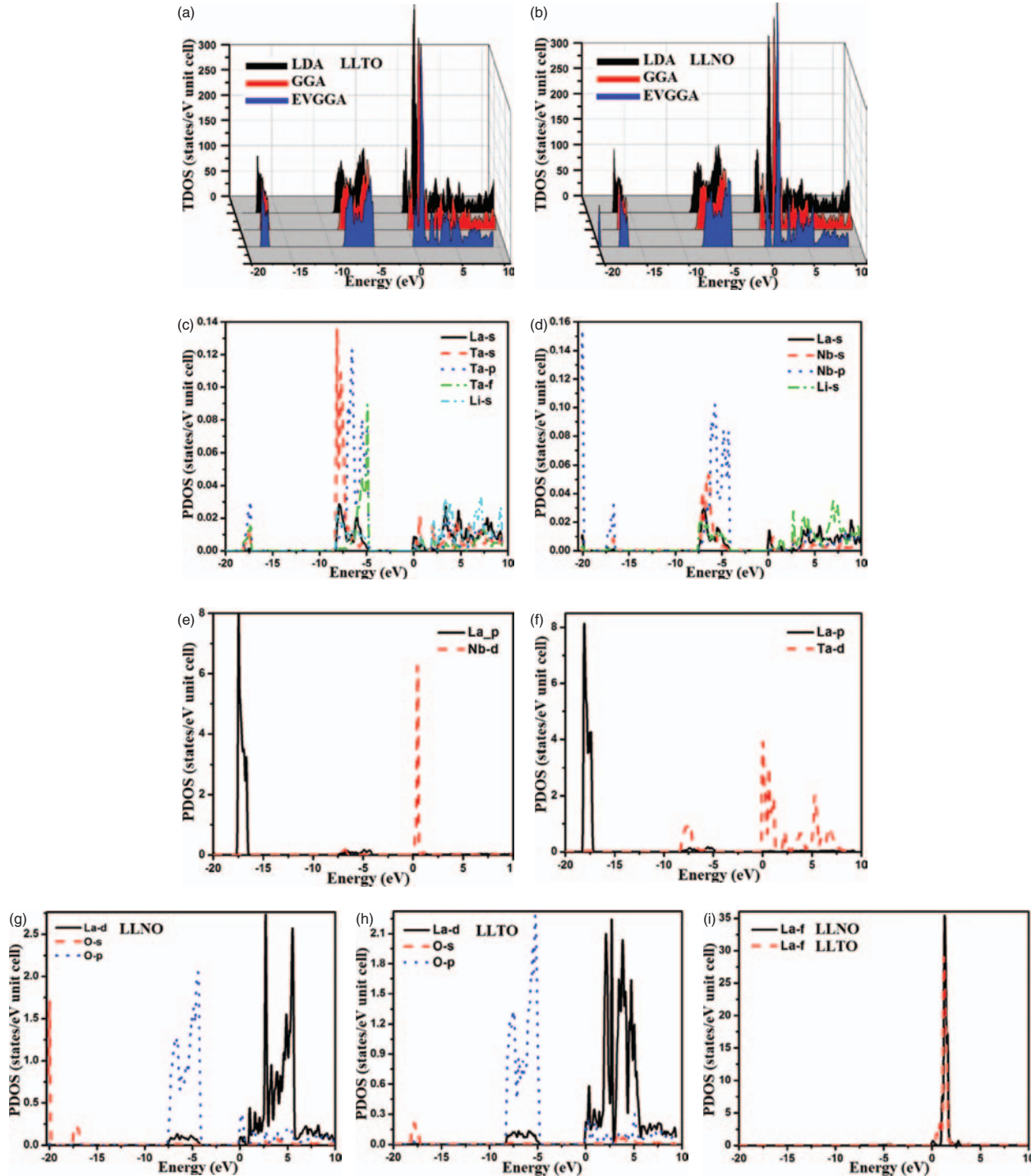


Fig. 3. Calculated total density states (DOS) and partial density of states (PDOS) for $\text{Li}_5\text{La}_3\text{Nb}_2\text{O}_{12}$ and $\text{Li}_5\text{La}_3\text{Ta}_2\text{O}_{12}$.

major contribution of intra-band transition (Drude term) to the imaginary part $\varepsilon_2(\omega)$ of the dielectric tensor is found below 1.0 eV for both compounds. Two maxima are observed in $\varepsilon_2(\omega)$ at 4.5 eV and 9.0 eV for LLNO compound and at 6.0 eV and 9.0 eV for LLTO compound, respectively. These are associated to the inter-band transitions from the O-p state (occupied band) to La-f state (unoccupied bands). The imaginary part $\varepsilon_2(\omega)$ of the

dielectric function tends to decrease at high energy beyond 10.0 eV for both compounds, due to the disorientation of the dipole under the high frequency electric field.

The real part $\varepsilon_1(\omega)$ of the dielectric tensor is obtained from the imaginary part $\varepsilon_2(\omega)$ of dielectric tensor by using the Kramers–Kronig transformation. One can see from Figure 5(b) that the Drude term is very significant in the energy range below than 0.7 eV at which the peaks vanish

Table II. Total density of states and electronic specific heat around Fermi level of $\text{Li}_5\text{La}_3\text{Nb}_2\text{O}_{12}$ and $\text{Li}_5\text{La}_3\text{Ta}_2\text{O}_{12}$.

$\text{Li}_5\text{La}_3\text{Nb}_2\text{O}_{12}$		
	$N(E_F)$ (states/eV)	γ (mJ/mol · K ²)
LDA	97.89	16.98
GGA	81.00	14.05
EVGGA	83.50	14.48
$\text{Li}_5\text{La}_3\text{Ta}_2\text{O}_{12}$		
	$N(E_F)$ (states/eV)	γ (mJ/mol · K ²)
LDA	82.77	14.35
GGA	74.20	12.87
EVGGA	72.00	12.49

for both compounds. In both compounds, the values of the real part $\varepsilon_1(\omega)$ of dielectric constant approach negative values (due to the plasma frequency, which explains the sum of the excitations) at energy greater than 9.0 eV. The plasma frequency is given by the following relation (taken from Ref. [22]):

$$\omega_p^2 = 4\pi n e^2 / m \quad (8)$$

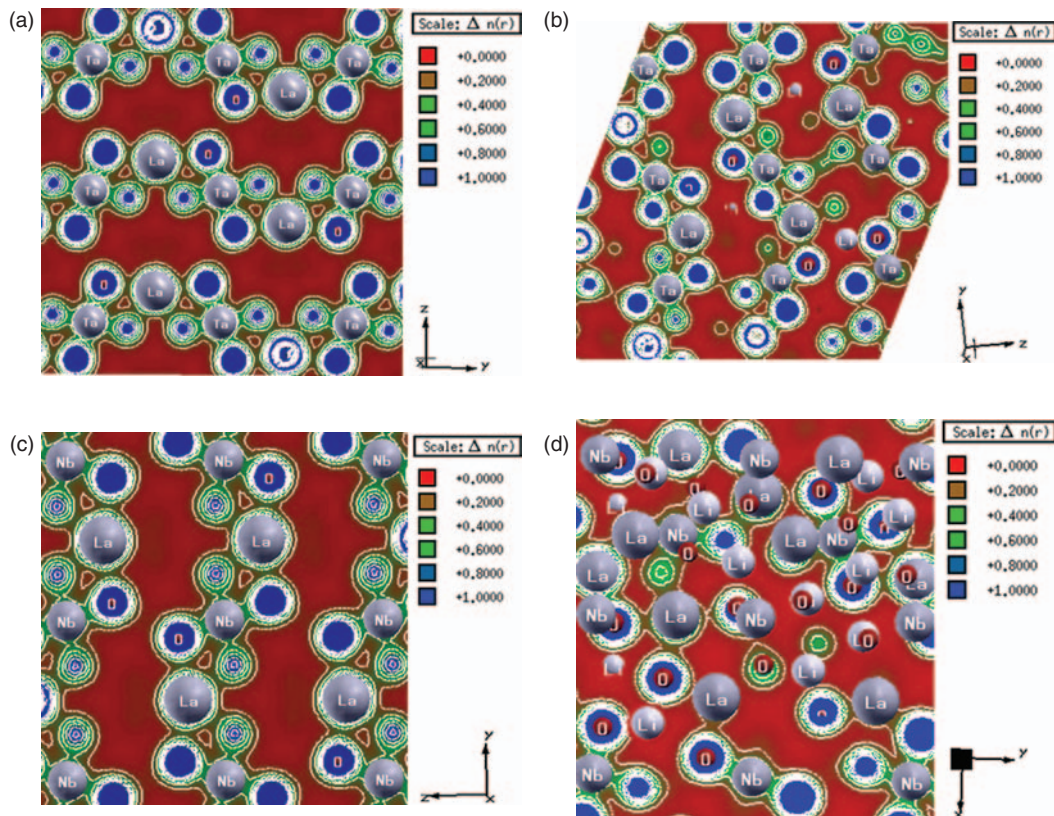
where n stands for the electron concentration, and m stands for the optical effective mass. Relation (2) gives an inverse proportionality between the optical effective mass

Table III. Calculated and experimental bond lengths of $\text{Li}_5\text{La}_3\text{Nb}_2\text{O}_{12}$, using EVGGA.

$\text{Li}_5\text{La}_3\text{Nb}_2\text{O}_{12}$		
Bond type	Bond lengths (Opt.) \AA^0	Bond lengths (Exp) \AA^0
Nb ₁ -O ₂	2.0300	1.9680
Nb ₂ -O ₁	2.0580	1.9715
La-O ₂	2.5900	2.5829
La-O ₁	2.5830	2.3819
Li-O ₁	2.1900	1.9286
Li-O ₂	1.9860	1.9262

and square of the plasma frequency, hence we get the ratio of the dispersion in the optical effective mass, which is given by $P = m_{xx}/m_{zz} = (\omega_p^{xx}/\omega_p^{zz})^2$ in one system and n is consider to be constant. P is a dimensionless quantity which explains anisotropic strength of a system, which the system showing isotropic nature for $P = 1$. The propagation of the incident photon energy (electromagnetic radiation) takes place in the energy range from 0.5 to 9.0 eV, where $\varepsilon_1(\omega) > 0$, and the photons show damping when $\varepsilon_1(\omega) < 0$ at energy greater than 9.0 eV, as shown in the Figure 5(b). From Figure 5(b) it is also noticed that the portion where $\varepsilon_1(\omega) = 0$, the incident photon energy $\hbar\omega$ present the polarization along the longitudinal direction.

The frequency dependent reflectivity $R(\omega)$ is shown in Figure 5(c). Due to the variation of energy the reflectivity

**Fig. 4.** Electronic space charge density distribution contour calculated with EVGGA in the (010) and (100) planes for $\text{Li}_5\text{La}_3\text{Nb}_2\text{O}_{12}$ and $\text{Li}_5\text{La}_3\text{Ta}_2\text{O}_{12}$.

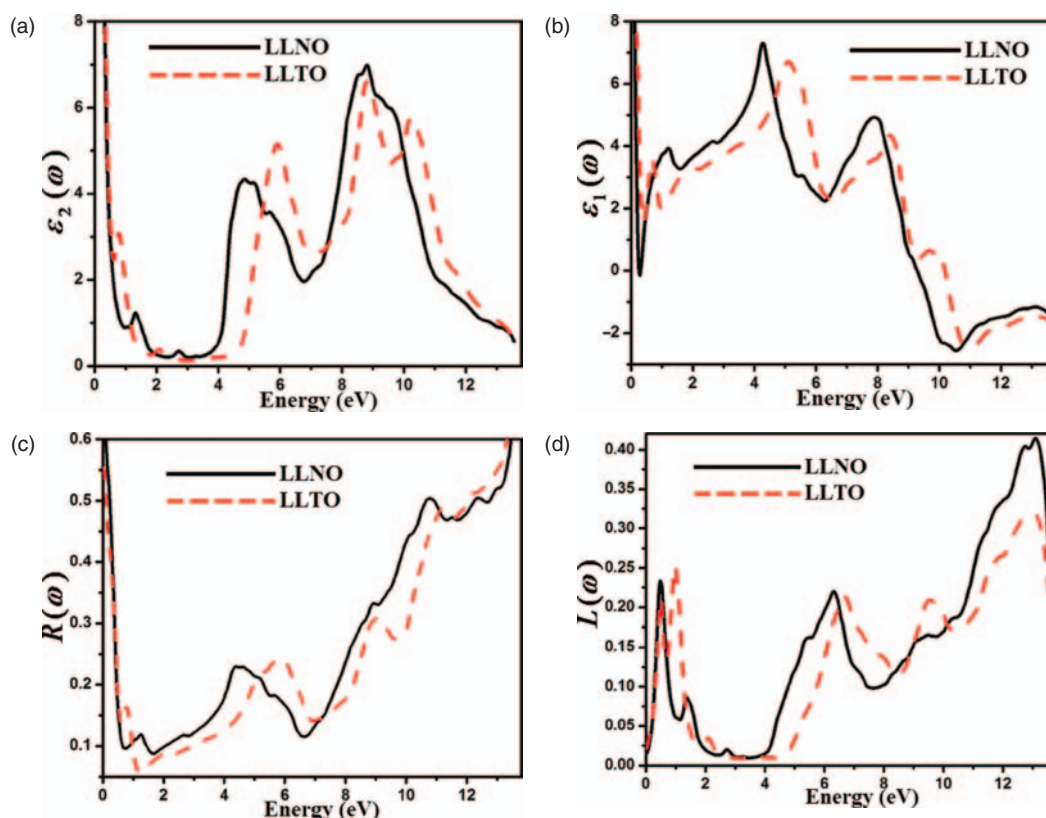


Fig. 5. Calculated real and imaginary part of dielectric function, reflectivity, energy loss function of $\text{Li}_5\text{La}_3\text{Nb}_2\text{O}_{12}$ and $\text{Li}_5\text{La}_3\text{Ta}_2\text{O}_{12}$, using EVGGA.

spectra of both compounds also show variation along the spectral region with a maximum value of 60% of reflectivity at 13.8 eV (UV region). It is clear from Figure 5(c) that the minimum value of reflectivity occurs in the visible region (from 1.1 to 2.0 eV), which demonstrates that both compounds are transparent and hence can be used as anti-reflecting coating materials for the incident electromagnetic radiations in this region. A dispersive nature is found in the reflectivity spectra of both compounds (Fig. 5(c)).

Figure 5(d) presents the energy loss function $L(\omega)$ as a function of energy. Generally, the energy loss curves are used to explain the fast traveling electron energy loss in the materials. The compound LLNO shows three main peaks at the energies 0.5 eV, 6.0 eV and 13.0 eV and the compound LLTO exhibit also three main peaks at the energies 1.0 eV, 6.8 eV and 13.0 eV, respectively (Fig. 5(d)). These peaks in the spectra correspond to the plasmon resonance or plasma oscillation with the decreasing energy of electrons instead of surface plasmon loss. The peaks in the energy loss spectra of both compounds are due to change from negative to positive value in the real part of the dielectric tensor (Fig. 5(b)), authenticating the transition from the metallic to dielectric character. The minimum value of the energy loss function between any two peaks corresponds to the increase in the energy of electrons as well as to the variation in the probability of plasmon oscillation. At higher energies an abrupt decrease is

reported in the energy loss function of both compounds (Fig. 5(d)).

3.3. Thermoelectric Properties

In this part of our research work, we have calculated the electronic transport properties including electrical conductivity, thermal conductivity, Seebeck co-efficient, power factor and heat capacity for the relaxed geometry of both LLNO and LLTO compounds as a function of temperature using BoltzTraP code,¹² as illustrated in Figure 6.

The temperature dependent electrical conductivities $\sigma(T)$ from 150 K to 800 K are illustrated in Figures 6(a), (b). The electrical conductivity of LLNO increases linearly with temperature up to 400 K, while the electrical conductivity of LLTO increases from 400 K. Beyond 400 K, the LLNO compound exhibits an exponential increase in the electrical conductivity²³ with temperature and gains the largest value of about $4.47 \times 10^{18} (\Omega\text{ms})^{-1}$ at 800 K. On the other hand, the LLTO compound features an increase in the electrical conductivity at higher temperature beyond 400 K and reaches its maximum value ($5.8 \times 10^{16} (\Omega\text{ms})^{-1}$) at 800 K (Fig. 6(b)). A significant dispersion is found in the electronic conductivity of both compounds (Figs. 6(a), (b)). Figure 6(a) shows that $\sigma(T)$ of LLNO decreases above 600 K and reaches a stationary level at higher temperature (800 K), corresponding to the decrease of charge carrier mobility. The reduction in

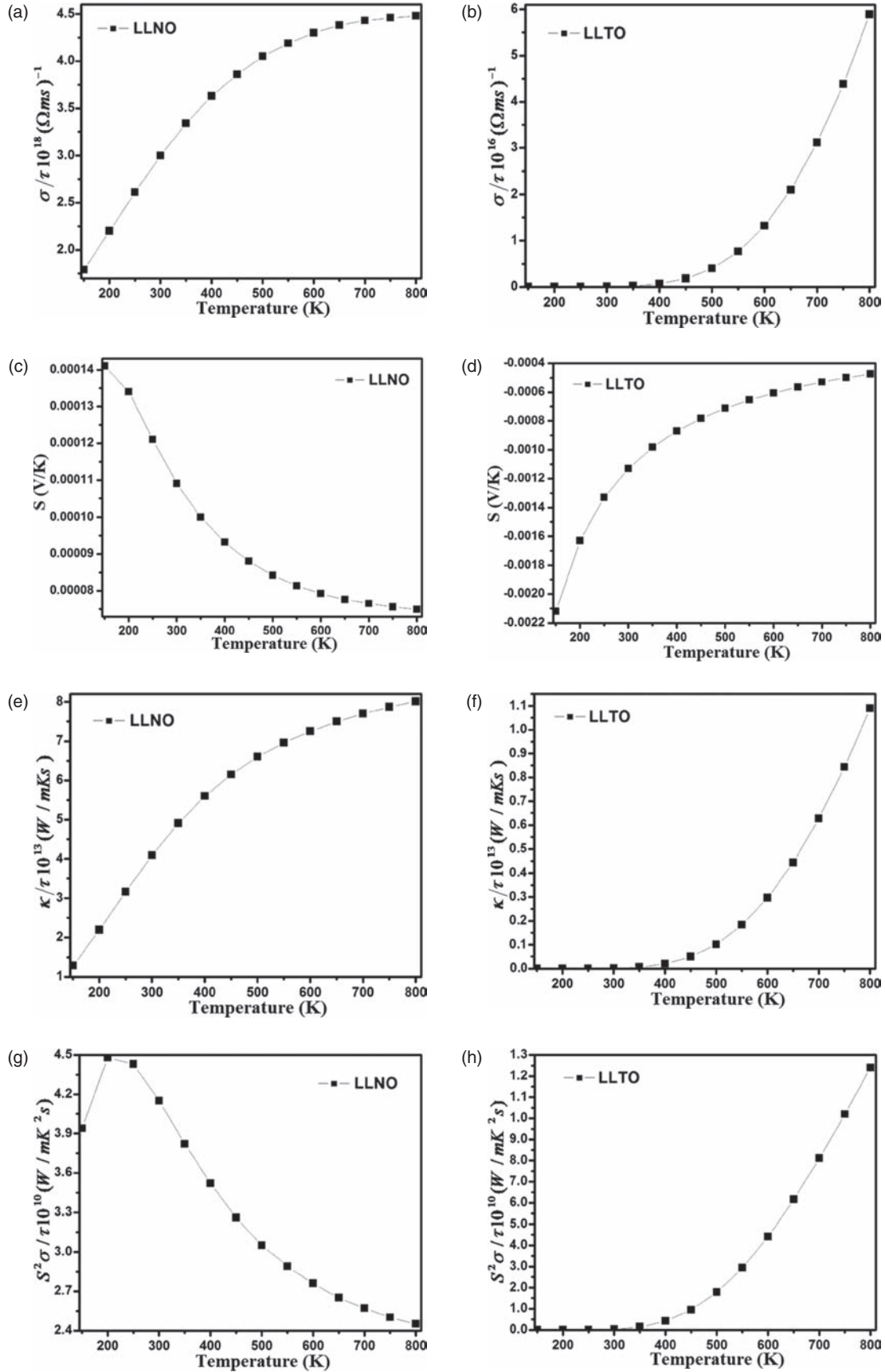


Fig. 6. Continued.

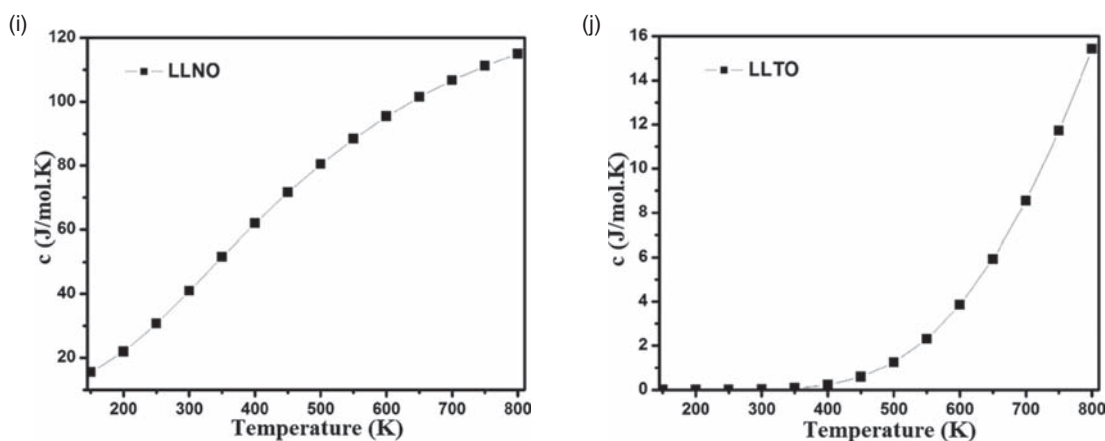


Fig. 6. Calculated transport coefficients of $\text{Li}_5\text{La}_3\text{Nb}_2\text{O}_{12}$ and $\text{Li}_5\text{La}_3\text{Ta}_2\text{O}_{12}$, as a function of temperature: electrical conductivity, Seebeck coefficient, thermal conductivity, power factor and heat capacity.

the mobility of both charge carriers (electrons and holes) is caused by the intrinsic defect concentration and thermal scattering of defects, which increases with temperature. From the plot in Figure 6(b), we concluded that the compound LLTO behaves like a degenerate semiconductor, because its electrical conductivity ($\sigma(T)$) increases with temperature, intrinsic defect density as well as defect scattering. At this point it should be recalled that our investigated compounds are electrolyte substances used in solid state batteries for which both ions and electrons take part in conduction. Here in these oxides Li^+ (cation) exhibits intrinsic Schottky defects indicate small ionic conductivity, but the electronic conductivity ($\sigma(T)$) is promising.

Figures 6(c), (d) show the calculated Seebeck coefficient $S(T)$ as a function of temperature ranging from 150 K to 800 K. In our investigated compounds, the magnitude of Seebeck coefficient ($S(T)$) also depends on the movable charge carriers and the intrinsic defect concentration.

Mathematically, the charge carrier concentration and density of states dependent Seebeck coefficient can be written as;

$$S = \frac{\pi^2 k_B^2 T}{3q} \frac{N(E)}{n} \Big|_{E=E_F} \quad (9)$$

From the above Eq. (3), it is clear that Seebeck coefficient is inversely proportional to the carrier concentration and mobility of charge carrier.

The Seebeck coefficient of LLNO compound decreases exponentially from its maximum value 0.00014 (V/K) to minimum value 0.0007 (V/K) with temperature up to 800 K (Fig. 6(c)), while the Seebeck coefficient of the compound LLTO increases exponentially with temperature and gain its maximum value -0.0006 (V/K) at 800 K (Fig. 6(d)). The variations are due to the fact that at higher temperature, the compound LLTO (n -type doped material) is characterized by lower Seebeck coefficient and higher carrier concentration according to Eq. (3). On the other hand, the compound LLNO (p -type doped material) has degenerate semiconductor-like behavior, in which

the Seebeck coefficient exhibits an increase, due to the increase in both carrier concentration and intrinsic vacancies with temperature. Following Figures 6(c), (d) the Seebeck coefficient of both compound exhibit different temperature dependence. From Figures 6(c), (d), one can clearly observe that the LLTO is good thermoelectric material as compared to LLNO because the former has negative value of Seebeck coefficient (increases with temperature) and later compound decreases with temperature.

Figures 6(e), (f) shows the thermal conductivity $\kappa(T)$ of both compounds versus temperature (150 to 800 K), including the contribution of electrons, which is estimated by using the familiar Wiedemann–Franz law:

$$\kappa_{el} = L_0 \sigma T \quad (10)$$

where L_0 stands for the Lorentz number, its value being equal to $2.45 \times 10^{-8} \text{ V}^2 \text{ K}^2$, which is assumed to be constant for metals and semiconductor. Thermal conductivity $\kappa(T)$ of LLNO compound is around 0.4×10^{13} (W/mKs) at 150 K, while it is zero for the LLTO compound up to 350 K (Figs. 6(e), (f)).

Following Figures 6(e) (f) the thermal conductivity $\kappa(T)$ of both compounds (LLNO and LLTO) increases due to the increase in temperature from 150 K to 800 K. The compound LLNO possesses thermal conductivities of about 8×10^{13} (W/mKs) and approaching the stable position, while $\kappa(T)$ of the compound LLTO is predicted to approach an ever increasing value of 1.1×10^{13} (W/mKs) at 800 K, as illustrated in Figures 6(e), (f). The increase in the thermal conductivities with temperature is mainly caused by the electron contributions, because the electrons close to the Fermi level can jump to t vacant states by acquiring very small energy, hence reaching states above the Fermi level. The intrinsic defects also affect thermal conductivity $\kappa(T)$ because at low temperature they provide negligible contribution to $\kappa(T)$, while at high temperature the concentration of intrinsic defects also increases, resulting in greater thermal conductivity (Figs. 6(e), (f)).

We emphasize that the intrinsic cationic defects effectively interact with the phonon sub-system.²⁴

The power factor $S^2\sigma(T)$ of LLNO and LLTO compounds as a function of temperature is presented in Figures 6(g), (h). The LLNO compound shows a maximum value of 4.4×10^{10} ($\text{W/mK}^2\text{s}$) which then decreases with the increase in the temperature until it reaches its minimum value of 2.475×10^{10} ($\text{W/mK}^2\text{s}$) at 800 K. It is also obvious from Figure 6, that the power factor $S^2\sigma(T)$ of LLTO compound starts from 325 K and reaches its maximum value 1.24×10^{10} ($\text{W/mK}^2\text{s}$) at 800 K, beyond which it further increases. The LLTO shows a dramatic increase in thermoelectric performance at high temperature as compared to LLNO. This maximum value of power factor $S^2\sigma_{\text{max}}$ is good for the practical thermoelectric materials. According to the electrical conductivity $\sigma(T)$ and Seebeck coefficient $S(T)$, which depend on the carrier concentration, it is obvious that the power factor ($S^2\sigma(T)$) for such complex oxides increases based on the following three points:

- (1) the increase in the density of states around the Fermi level
- (2) increase in the time between collisions
- (3) the reduction of charge carrier effective mass.

To evaluate thermoelectric performance of both compounds more clearly, we use the figure of merit ZT , given by:

$$ZT = \frac{S^2\sigma T}{\kappa} \quad (11)$$

where S , σ , κ and T stands for Seebeck coefficient, electrical conductivity, thermal conductivity and temperature. The calculated figure of merit (ZT) of both compounds are listed in Table IV. From the calculated data, one can see that at low temperature n -type doped compound exhibits higher value of ZT than the p -type doped compound, which instead exhibit greater value of ZT at 300 K. As discussed above, the thermal conductivity depends on carrier as well as intrinsic defect concentration, which increases with temperature. According to relation (10), a greater thermal conductivity result in smaller ZT value. LLTO compound (n -type) presents $ZT \approx 1$ at 450 K, which shows that it should exhibit efficient thermoelectric performance at this temperature. On the other hand, LLNO compound (p -type) indicates greater ZT value (0.025) at 800 K. In comparison, LLTO compound is very good candidate for thermoelectric power generation and possess maximum thermoelectric performance as compared to LLNO compound.

Figures 6(i), (j) shows the variation of heat capacity as a function of temperature for both compounds. The Debye formula for the specific heat at constant pressure per atom of a compound is given by:

$$c_p(T; T_D, A) = A \left(\frac{T}{T_D} \right)^3 \int_0^{T_D/T} \frac{x^4 e^x}{(e^x - 1)^2} dx \quad (12)$$

Table IV. Calculated hermoelectric figures of merit.

Compound name	T (K)	σ/τ ($\Omega \text{ ms}^{-1}$)	S/τ (V/K)	κ/τ (W/mKs)	ZT
LLNO	150	1.78×10^{18}	1.14×10^{-4}	1.27×10^{13}	4.18×10^{-1}
	200	2.19×10^{18}	1.33×10^{-4}	2.18×10^{13}	3.59×10^{-1}
	250	2.61×10^{18}	1.21×10^{-4}	3.16×10^{13}	3.02×10^{-1}
	300	2.99×10^{18}	1.09×10^{-4}	4.09×10^{13}	2.62×10^{-1}
	350	3.34×10^{18}	1.00×10^{-4}	4.91×10^{13}	2.38×10^{-1}
	400	3.63×10^{18}	9.31×10^{-5}	5.59×10^{13}	2.25×10^{-1}
	450	3.86×10^{18}	8.80×10^{-5}	6.15×10^{13}	2.18×10^{-1}
	500	4.04×10^{18}	8.41×10^{-5}	6.60×10^{13}	2.17×10^{-1}
	550	4.19×10^{18}	7.92×10^{-5}	6.96×10^{13}	2.19×10^{-1}
	600	4.30×10^{18}	7.83×10^{-5}	7.25×10^{13}	2.23×10^{-1}
	650	4.37×10^{18}	7.76×10^{-5}	7.50×10^{13}	2.28×10^{-1}
	700	4.42×10^{18}	7.64×10^{-5}	7.69×10^{13}	2.35×10^{-1}
750	4.46×10^{18}	7.56×10^{-5}	7.87×10^{13}	2.43×10^{-1}	
800	4.47×10^{18}	7.49×10^{-5}	8.01×10^{13}	2.51×10^{-1}	
LLTO	150	1.19×10^8	-2.16×10^{-3}	8.38×10^4	0.995235
	200	5.10×10^{10}	-1.66×10^{-3}	2.84×10^7	0.990766
	250	2.02×10^{12}	-1.36×10^{-3}	9.37×10^8	0.995695
	300	2.38×10^{13}	-1.15×10^{-3}	9.54×10^9	0.990041
	350	1.40×10^{14}	-1.00×10^{-3}	4.94×10^{10}	0.989165
	400	5.27×10^{14}	-8.87×10^{-4}	1.67×10^{11}	0.990851
	450	1.48×10^{15}	-7.98×10^{-4}	4.28×10^{11}	0.989423
	500	3.37×10^{15}	-7.26×10^{-4}	9.00×10^{11}	0.997730
	550	6.62×10^{15}	-6.67×10^{-4}	1.64×10^{12}	0.985730
	600	1.16×10^{16}	-6.17×10^{-4}	2.69×10^{12}	0.983411
	650	1.86×10^{16}	-5.76×10^{-4}	4.08×10^{12}	0.980770
	700	2.78×10^{16}	-5.40×10^{-4}	5.81×10^{12}	0.977823
750	3.94×10^{16}	-5.09×10^{-4}	7.87×10^{12}	0.974593	
800	5.34×10^{16}	-4.83×10^{-4}	1.02×10^{13}	0.97100	

where T_D stands for the Debye temperature, and A is a constant. Both T_D and A are obtained for each compound from their heat capacity at 298 K, while c_p at 298 K is given by:

$$c_p(298; T_D, A) = c_p, 298 \text{ K} \quad (13)$$

This relation means that c_p is calculated at 298 K by integration of the additional parameters, such as T_D and A . At high temperature, the heat capacity of LLNO compound approaches the classical constant value of $6R$, where R is molar gas constant. At low temperature up to 350 K, the heat capacity of both compounds show greater dispersion (Figs. 6(i), (j)). This type of underestimation in the high temperature range has also been found in the all-electron calculation.²⁵

The heat capacity of LLNO compound shows sharp increase up to 400 K, thus obeying the law of T^3 which is understandable from basic excitation of phonons. It is also clear from Figures 6(i), (j) that the heat capacity of LLNO compound increases slowly at higher temperature, while for LLTO compound it starts raising at 400 K and then increases with increasing temperature up to 800 K. One can see from Figures 6(i), (j) that at 800 K temperature both compounds exhibit maximum values of specific heat capacity, which are due to the fact that all electrons get excited and occupy higher energy states and contribute to specific heat.

4. CONCLUSIONS

In summary, we have carried out the calculations of the electronic structure, electronic charge density, optical properties, and transport properties of the bulk garnet-like oxides $\text{Li}_5\text{La}_3\text{M}_2\text{O}_{12}$ ($\text{M} = \text{Nb, Ta}$), using the full-potential linearized augmented plane-wave (FPLAPW) technique and the semi-classical Boltzmann theory. Our calculations show that $\text{Li}_5\text{La}_3\text{Nb}_2\text{O}_{12}$ and $\text{Li}_5\text{La}_3\text{Ta}_2\text{O}_{12}$ possess large density of states near the Fermi level E_F , which demonstrates that these two compounds are good thermoelectric materials. We used three approximations i.e., LDA, GGA and EVGGA for the exchange correlation (XC) potential. We have calculated the electronic charge density in the (100) and (010) crystallographic planes and found that the bonds exhibit greater dominance of the ionic character. We have investigated the optical properties, including the real and imaginary parts of the dielectric function, reflectivity and energy loss function on the basis of electronic structure. Our calculation indicates 60% reflection for incident electromagnetic radiation in the UV region. Our investigated compounds thus indicate high reflectivity and are anticipated to be good electrical conductors, which clearly shows the correlation between optical and thermoelectric properties. From the calculated electronic structure of such compounds having sub-bands due to the intrinsic defects, we found that the thermoelectric properties are increased due to the carrier and defect concentration, which also affects the optical properties. We also calculated the heat capacity using the BoltzTraP code at constant pressures for different temperatures ranging from 150 K to 800 K. We also confirm the degenerate semiconductor-like nature of LLTO from the calculated temperature dependent electronic conductivity. Our results for the power factor $S^2\sigma(T)$ show that LLTO is more appropriate as thermoelectric materials than LLNO, because it shows dramatic increases in $S^2\sigma(T)$ with temperature.

Acknowledgment: This result was developed within the CENTEM project, Reg. no. CZ.1.05/2.1.00/03.0088, co-funded by the ERDF as part of the Ministry of Education, Youth and Sports OP RDI program. School

of Material Engineering, Malaysia University of Perlis, Malaysia.

References and Notes

1. A. D. Robertson, A. R. West, and A. G. Ritchie, *Solid. State. Sci.* 13, 1760 (2011).
2. G. A. Adachi, N. Imanaka, and H. Aono, *Adv. Mater.* 8, 127 (1996).
3. (a) O. Bohnke, C. Bohnke, and J. L. Fourquet, *Solid. State. Ionics.* 91, 21 (1996); (b) P. Birke, S. Scharner, R. A. Huggins, and W. Weppner, *J. Electrochem. Soc.* 144, L167 (1997).
4. C. H. Chen and K. Amine, *Solid. State. Ionics* 144, 51 (2001).
5. V. Thangadurai, S. Adams, and W. Weppner, *Chem. Mater.* 16, 2998 (2004).
6. V. Thangadurai and W. Weppner, *Mater. Res. Bull.* 43, 765 (2008).
7. (a) B. J. Neudecker and W. Weppner, *Mater. Sci. and Engg.: B* 143, 14 (2007); (b) X. Yu, J. B. Bates, G. E. Jellison, and F. X. Hart, *Solid. State Ionics.* 179, 1666 (2008).
8. V. Thangadurai, H. Kaack, and W. Weppner, *J. Am. Ceram. Soc.* 86, 437 (2003).
9. D. Mazza, *Mater. Ceramics. International* 40, 5043 (2014).
10. H. Hyooma and K. Hayashi, *Solid State Ionics* 253, 137 (2013).
11. V. Thangadurai, S. Adams, and W. Weppner, *Chem. Mater.* 16, 2998 (2004).
12. G. K. H. Madsen and D. J. Singh, *Comput. Phys. Commun.* 175, 67 (2006).
13. W. Kohn and L. J. Sham, *Phys. Rev. A* 140, 1133 (1965).
14. P. B. K. Schwarz, G. K. H. Madsen, D. Kvasnicka, and J. L. WIEN2K, An Augmented Plane Wave Plus Local Orbital, Program for Calculating Crystal Properties, Vienna University of Technology, Vienna, Austria, ISBN: 3-9501031-1-2 (2001).
15. K. Schwarz, P. Blaha, and G. K. H. Madsen, *Comput. Phys. Commun.* 147, 71 (2002).
16. P. Hohenberg and W. Kohn, *Phys. Rev. B* 136, 864 (1964).
17. W. Kohn and L. J. Sham, *Phys. Rev. A* 140, 1133 (1965).
18. F. Zerarga, A. Bouhemadou, R. Khenata, and S. Bin-Omran, *Sol. State. Sci.* 13, 1638 (2011).
19. J. Ziman, *Principles of the Theory of Solids*, 2nd edn., Cambridge University Press (1972).
20. T. J. Scheideman, C. Ambrosch-Draxl, T. Thonhauser, J. V. Badding, and J. O. Sofo, *Phys. Rev. B* 68, 125210 (2003).
21. G. D. Mahan, *Intern. Tables for Crystall. D* 220 (2006).
22. N. W. Ashcroft and N. D. Mermin, *Solid State Physics*, Holt Rinehart and Winston Inc., New York (1976), p. 18.
23. Y. Kumekawa, M. Hirai, Y. Kobayashi, S. Endoh, E. Oikawa, and T. Hashimoto, *J. Therm. Anal. Calorim.* 99, 57 (2010).
24. I. V. Kityk, M. Makowska-Janusik, M. D. Fontana, M. Aillerie, and A. Fahmi, *J. Phys. Chem. B* 105, 2242 (2001).
25. P. F. Weck, E. Kim, N. Balakrishnan, F. Poineau, C. B. Yeaman, and K. R. Czerwinski, *Chem. Phys. Lett.* 443, 82 (2007).